Tri-Phasing Modulation for Efficient and Wideband Radio Transmitters

Jerry Lemberg, *Student Member, IEEE*, Mikko Martelius, *Student Member, IEEE*, Marko Kosunen, *Member, IEEE*, Enrico Roverato , Kari Stadius, *Member, IEEE*, Lauri Anttila, *Member, IEEE*, Mikko Valkama, *Senior Member, IEEE*, and Jussi Ryynänen, *Senior Member, IEEE*

***Abstract*—In this paper, we show that amplitude transitions that are inherent to the multilevel outphasing radio transmitter architecture distort the transmitted signal due to time-domain discontinuities. In order to address this challenge, we propose a new transmitter architecture called tri-phasing which avoids discontinuities in signal waveforms and thus achieves significantly better linearity than multilevel outphasing. The output waveform in tri-phasing can be made continuous by representing the baseband signal with three components. One of the three components is amplified by discrete amplitude steps, whereas the other two are used to compensate the instantaneous shift in the output waveform due to the discrete amplitude step and to provide fine amplitude resolution. An implementation of the tri-phasing transmitter requires three phase modulators and additional digital signal processing. The system-level simulations performed in this paper demonstrate that the ACLR of a multilevel outphasing transmitter with 4 amplitude levels and 10-bit phase resolution is limited to -48 dBc, when simulated with a 100 MHz carrier-aggregated LTE downlink signal at 2.46 GHz carrier frequency. The proposed tri-phasing transmitter achieves -58 dBc ACLR with the same simulation parameters, indicating that continuous amplitude transitions can significantly improve the transmitter linearity.**

***Index Terms*—Outphasing, digital, interpolation, phase modulator, phase modulation, DIPM, switch-mode PA, tri-phasing, transmitter, CMOS**

I. Introduction

THE emerging 3GPP 5G New Radio (NR) standard [1] aims to increase the capacity of existing cellular networks below 6 GHz frequency bands by employing up to 100 MHz modulation bandwidth. Further advances to be expected in the near future will include more complex modulation schemes and large-scale antenna systems [2], [3]. As a consequence, radio transmitters based on conventional architectures are facing significant challenges to cope with the requirements set by 5G. One such challenge is that the transmitter generates spectrally efficient signals with high peak-to-average power ratios (PAPR), which leads to low power efficiency with conventional linear power amplifiers (PA). However, highly efficient but non-linear switch-mode PAs (SM-PA) can be used to improve the transmitter chain efficiency. Efficient polar [4]–[10] and outphasing [11]–[18] transmitters inherently utilize constant-envelope phase-modulated signals and thus are capable of employing SM-PAs.

Manuscript received October 27, 2017; revised March 14, 2018.

J. Lemberg (e-mail: jerry.lemberg@aalto.fi), M. Martelius, M. Kosunen, E. Roverato, K. Stadius and J. Ryynänen are with the Department of Electronics and Nanoengineering, School of Electrical Engineering, Aalto University, Espoo, Finland

L. Anttila and M. Valkama are with the Department of Electronics and Communications Engineering, Tampere University of Technology, Tampere, Finland

This work is supported by Nokia, the Finnish Funding Agency for Technology and Innovation, the Academy of Finland under project No. 301820 and the European Union's Horizon 2020 research and innovation programme under the Marie Sklodowska-Curie grant agreement No. 704947.

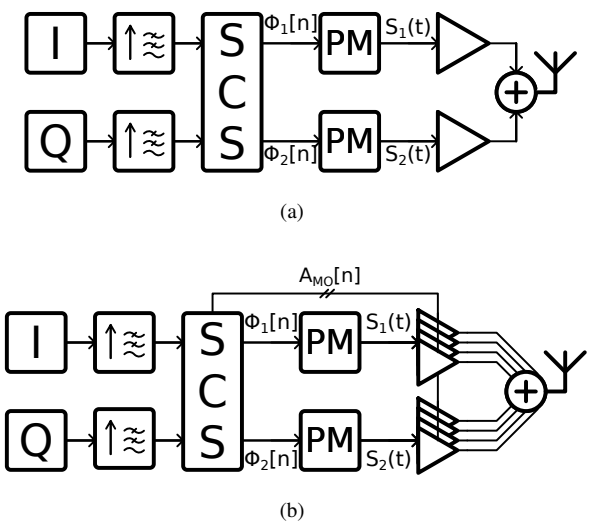

Fig. 1. Block diagrams of (a) an outphasing transmitter and (b) a multilevel outphasing transmitter.

Polar transmitters can achieve very high efficiency by modulating the supply voltage of SM-PAs to generate amplitude modulation. However, due to limited bandwidth of supply modulators, achieved signal bandwidths have been limited to a few tens of megahertz [4], [5]. Alternatively, Fig. 1(a) shows the schematic of an outphasing transmitter that utilizes two phase modulators (PM) to achieve phase and amplitude modulation. The baseband signal processing includes interpolating the Cartesian signal to a sufficiently high sample rate and conversion into phase domain in the signal component separator (SCS) that controls the PMs. By avoiding bandwidth limited supply modulators, outphasing moves the amplitude modulation bandwidth requirements to the phase modulators, potentially enabling wider signal bandwidth. Digital-intensive phase modulators have been demonstrated to operate with sample rates up to 2.4 GHz [15], which is sufficient for phase modulation with more than 100 MHz signal bandwidth when taking bandwidth expansion into account [6]. However, the efficiency of a wideband outphasing transmitter utilizing class-

D SM-PAs also degrades quickly in power back-off [19], thus resulting in poor efficiency with high PAPR signals. Fig. 1(b) shows the schematic of a multilevel outphasing transmitter, which has been proposed as a solution to improve the efficiency of outphasing transmitters [20], [21]. Compared to conventional transmitters, multilevel outphasing has potential to significantly increase the efficiency of the complete transmitter chain with efficient use of SM-PAs, while simultaenously enabling wide signal bandwidth. However, only a few CMOS implementations [22]–[25] and high power demonstrators [26]–[28] have been published. Among these, the journal publications [22], [23], [28] reported distortion originating from the amplitude transitions in multilevel operation. Moreover, publications on multilevel outphasing typically focus on the efficiency improvement of the architecture with moderate bandwidth signals. Hence, no detailed analysis exists about the fundamental linearity limitations of multilevel outphasing.

In this paper, we show that discrete-time amplitude transitions in multilevel outphasing significantly distort the transmitted signal. As a consequence, the transmitter linearity becomes limited by the distortion instead of its phase resolution characteristics. In order to overcome this limitation and improve the performance of multilevel transmitters that utilize phase modulation, we propose a new transmitter architecture called tri-phasing. The tri-phasing signal composition enables significant improvement in transmitter linearity as discontinuities in the output waveform near amplitude transitions can be avoided. Tri-phasing enables comparable efficiency as multilevel outphasing, with the additional overhead of a third phase modulator and more complex digital signal processing. Tri-phasing thus improves over the multilevel outphasing transmitter linearity to meet the stringent adjacent channel leakage ratio (ACLR) requirements for basestation applications with sufficient margin. As a result, tri-phasing can provide an alternative to the conventional quadrature transmitter architecture, and the capability to use SM-PAs helps to improve the complete transmitter chain efficiency.

A robust implementation of the tri-phasing transmitter requires that the amplitude transitions are accurately synchronized to the phase-modulated signals. Achieving this synchronization requires the ability to define the edges of the square-wave phase-modulated RF signals independently within the sample period. We have presented the digital interpolating phase modulator (DIPM) concept in [29] and a prototype implementation in [30], which we propose to be used as phase modulators also in the tri-phasing transmitter. The DIPM independently defines each rising and falling edge of the phase-modulated signal, which is achieved by linearly interpolating the phase signal with solvers in digital domain, and reconstructing the square-wave RF signal by toggling it accurately within the sample period. The tri-phasing concept requires DIPM solvers to be modified from what was presented in [29] and therefore also the required digital signal processing (DSP) for tri-phasing is described in this paper.

This paper is organized as follows: In Section II, we describe relevant background information related to outphasing and phase modulator architectures. In Section III, we analyze the challenges associated with multilevel outphasing. In Section IV, we introduce the tri-phasing architecture as a solution to overcome the performance degradation of multilevel outphasing. In Section V, the performance of the tri-phasing transmitter is demonstrated with system-level simulations and compared against the conventional multilevel outphasing transmitter. Section VI concludes the paper.

II. Background

In order to provide sufficient background information to demonstrate the research problem and our solution to it, we first present the concept of multilevel outphasing and provide an overview of the two phase modulator architectures considered in this paper.

A. Outphasing and Multilevel Outphasing

The amplitude and phase-modulated signal $V(t)$ is given in polar form as

$$V(t) = r(t)\cos\left(\omega_c t + \phi(t)\right), \quad r(t) \in [0,1] \tag{1}$$

where ω_c is the angular carrier frequency and $r(t)$ and $\phi(t)$ correspond to the normalized envelope and phase of the complex baseband data signal, respectively. In outphasing, $V(t)$ is divided into two constant-envelope outphasing signal components $S_1(t)$ and $S_2(t)$ as

$$V(t) = \frac{1}{2}\left(S_1(t) + S_2(t)\right) \tag{2}$$

$$S_{1,2}(t) = \cos(\omega_c t + \Phi_{1,2}(t)) \tag{3}$$

$$\Phi_1 = \phi(t) + \theta(t) \tag{4}$$

$$\Phi_2 = \phi(t) - \theta(t), \tag{5}$$

where the outphasing angle $\theta(t)$ is calculated from the normalized polar signal radius $r(t)$ with

$$\theta(t) = \arccos(r(t)). \tag{6}$$

The derivation of conventional outphasing can be extended to multilevel outphasing as

$$V(t) = \frac{A_{MO}(t)}{2A_{max}}\left(S_1(t) + S_2(t)\right)$$
$$A_{MO}(t) \in \{1, 2, 3 ... A_{max}\}, \tag{7}$$

where $A_{MO}(t)$ represents the discrete amplitude level. Assuming equally spaced amplitude levels up to integer level A_{max}, $A_{MO}(t)$ and the outphasing angle $\theta_{MO}(t)$ are calculated as

$$A_{MO}(t) = \lceil r(t)A_{max} \rceil \tag{8}$$

$$\theta_{MO}(t) = \arccos\left(\frac{r(t)A_{max}}{A_{MO}(t)}\right). \tag{9}$$

B. Digital Phase Modulator Architectures for Outphasing

1) Sample-and-Hold Phase Modulator (SH-PM): The conventional sample-and-hold phase modulator performs phase modulation by delaying the square-wave local oscillator (LO) waveform with a phase offset corresponding to the modulating phase as

$$S(t) = \mathrm{sgn}\left(\cos\left(\omega_c t + \Phi_{sh}(t)\right)\right), \tag{10}$$

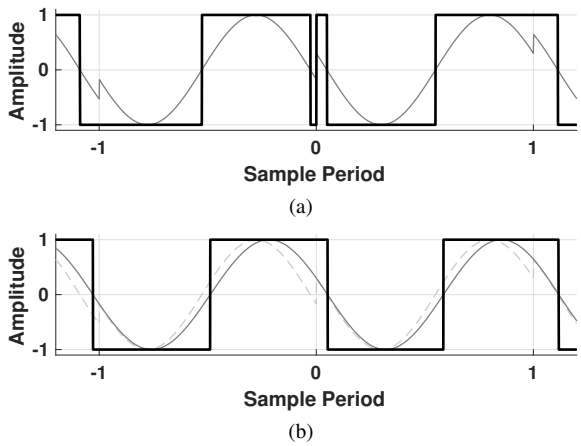

Fig. 2. (a) Origin of narrow pulses with the SH-PM demonstrated with sinusoidal and square-wave carriers. (b) Same signal with the DIPM, demonstrating how phase interpolation prevents generation of narrow pulses.

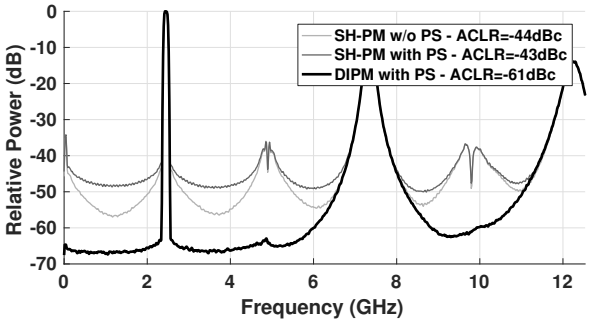

Fig. 3. Spectrum of a 100 MHz signal at 2.46 GHz center frequency with an outphasing transmitter using the SH-PM, with and without pulse swallowing (PS), and the DIPM with pulse swallowing.

where $\Phi_{sh}(t)$ is the sampled-and-held modulating phase signal, and the signal is sampled once each LO period. The time-domain waveform of the SH-PM is depicted in Fig. 2(a) with both sinusoidal and square-wave signals. The sinusoidal signal reveals the fundamental problem in the architecture, as the waveform of $S(t)$ exhibits discontinuities when the value of $\Phi_{sh}(t)$ changes abruptly at sample period boundaries. As explained in [29] and illustrated in Fig. 2(a), the SH-PM may generate narrow pulses that cannot be reproduced by the PAs. These narrow pulses are thus swallowed and the phase-modulated signal becomes distorted, which ultimately degrades the linearity of the outphasing transmitter. Furthermore, sampling images of $\Phi_{sh}(t)$ intermodulate with the square-wave carrier harmonics, which shifts the sampling images in frequency onto the signal band, and thus limits the achievable adjacent channel leakage ratio (ACLR) of the transmitter [29], [31].

2) Digital Interpolating Phase Modulator (DIPM): The concept of digital phase interpolation has been proposed as a potential solution to improve the phase-modulated signal sampling image suppression [29], [31]. In [29], we introduced a new digital interpolating phase modulator (DIPM) architecture, where the total phase $\rho(t) = \omega_c t + \phi(t) \pm \theta(t)$ is linearly interpolated between two consecutive discrete samples in digital domain. Fig. 2 demonstrates the difference between the DIPM and the SH-PM in time domain. The linear interpolation ensures that uncontrollably narrow pulses are not generated within the phase modulator. An even more significant benefit of the DIPM is that the sampling images of the phase signal $\rho(t)$ are suppressed by sinc^2 response in contrast to the sinc response of SH-PM, improving transmitter linearity and thus ACLR [29], [31].

The phase interpolation with DSP can be explained as follows: A continuous-time outphasing signal can be presented in continuous and discrete-time as

$$\rho(t) = \omega_c t + \phi(t) \pm \theta(t) \tag{11}$$

$$\rho[n] = n\alpha + \phi[n] \pm \theta[n], \tag{12}$$

where α signifies the constant phase increment, defined by the ratio of the carrier frequency f_c and the transmitter sample rate F_s as

$$\alpha = 2\pi \frac{f_c}{F_s}. \tag{13}$$

Thus, the value of α defines the carrier frequency, and enables digital carrier generation on a desired frequency.

The phase interpolation is performed with a single linear interpolation between $\rho[n-1]$ and $\rho[n]$ by K values as

$$\rho_{int}[n,k] = \rho[n-1] + \frac{k}{K} \cdot \Delta\rho[n] \quad k \in \{1,2,3,...,K\} \tag{14}$$

$$\Delta\rho[n] = \alpha + \Delta\phi_{uw}[n] \pm \Delta\theta[n], \tag{15}$$

where the unwrapped polar phase difference $\Delta\phi_{uw}[n]$ is required to form the phase increment $\Delta\rho[n]$. The zero crossings X_i of the time-domain signal appear every integer multiple of π in the phase signal, and they are calculated as

$$\rho_{int}[n, X_i] = i\pi, \quad i \in \{0,1,2,\dots\} \tag{16}$$

A more detailed description of the operation of the DIPM, including implementation details, is presented in [29].

Fig. 3 shows the simulated spectra of the SH-PM and the DIPM, which are used in outphasing transmitters with a 100 MHz aggregated LTE downlink signal at 2.46 GHz carrier frequency. The figure reveals the significant improvement to the outphasing transmitter ACLR enabled by the DIPM, which notably attenuates the sampling images visible in the spectrum of the SH-PM. As mentioned earlier, the SH-PM may generate narrow pulses that cannot be reproduced by the PAs. This leads to pulse swallowing (PS) within the transmitter chain, which further degrades the transmitter linearity. Unless otherwise specified, pulse swallowing is always taken into account in the simulations presented in this paper. The pulse swallowing threshold is 80 ps, and thus all narrower pulses are swallowed from individual PA unit outputs.

III. Limitations of Multilevel Outphasing

This section provides analysis on the distortion caused by discrete amplitude level transitions in the multilevel outphasing architecture.

A. Harmonic Discontinuities

This section aims to show that the amplitude transitions in multilevel outphasing, when used with square-wave signals, generate unwanted discontinuities in the harmonics of the carrier. Due to these discontinuities, the spectral spread of the harmonics sets a limit on the transmitter linearity. The Fourier series representation of an ideal square-wave outphasing signal can be used to analyze the harmonics. Here we use the Fourier sine series and apply it to present a phase-modulated square-wave as

$$S_{sq}(t) = \sum_{n}^{\infty} \frac{4}{n\pi} \sin\left(n\left(\omega_c t + \phi(t) \pm \theta(t)\right)\right), \quad n \in \{1, 3, 5 \dots\}. \tag{17}$$

Thus, the square-wave outphasing signal can be expressed as

$$V_{sq}(t) = \frac{1}{2}\left(S_{sq,1}(t) + S_{sq,2}(t)\right), \tag{18}$$

from where it can be easily shown that the amplitude of the nth harmonic is proportional to

$$A(t, n) \propto \cos(n\theta(t)). \tag{19}$$

In multilevel outphasing, the amplitude of the harmonic is also dependent on the discrete amplitude level A_{MO}. As A_{MO} and θ_{MO}, as defined in (8) and (9), are dependent on the level of the signal envelope r, the nth harmonic amplitude can be expressed as

$$A(n, r) = A_0(n) A_{MO}(r) \cos\left(n\theta_{MO}\left(r\right)\right), \tag{20}$$

where $A_0(n)$ signifies the constant amplitude factor for the nth harmonic as

$$A_0(n) = \frac{1}{A_{max}} \frac{4}{n\pi}. \tag{21}$$

Equation (20) is depicted graphically in Fig. 4, where the third and fifth harmonic amplitudes are presented as a function of the fundamental amplitude, showing discontinuities at amplitude level boundaries.

In order to demonstrate the problem with time-domain signals, let us assume a constant-frequency square-wave signal $V_{sq}(t)$ with an amplitude transition, where the signal envelope $r(t)$ of the fundamental frequency component $V(t)$ remains equal before and after the transition. In such a case the amplitude level A_{MO} changes from A_1 to $A_1 + 1$ and the outphasing angle changes simultaneously from zero to θ_2 as

$$A = A_0 A_1 \cos 0 = A_0 (A_1 + 1) \cos\theta_2. \tag{22}$$

Thus, the outphasing angle after the transition is

$$\theta_2 = \arccos\left(\frac{A_1}{A_1 + 1}\right). \tag{23}$$

Such an amplitude transition is presented in Fig. 5, where the time-domain waveform remains constant for 100 periods before and after the transition. The transition is visible as an instantaneous change in the square-wave time-domain waveform $V_{sq}(t)$, and although the fundamental component $V(t)$ remains continuous before and after the transition, the harmonic components $V_3(t)$ and $V_5(t)$ have discontinuities in phase and amplitude.

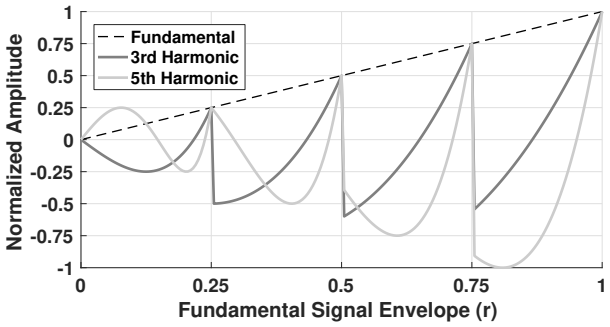

Fig. 4. Normalized amplitudes of the third and fifth harmonic components as a function of the fundamental amplitude in multilevel outphasing.

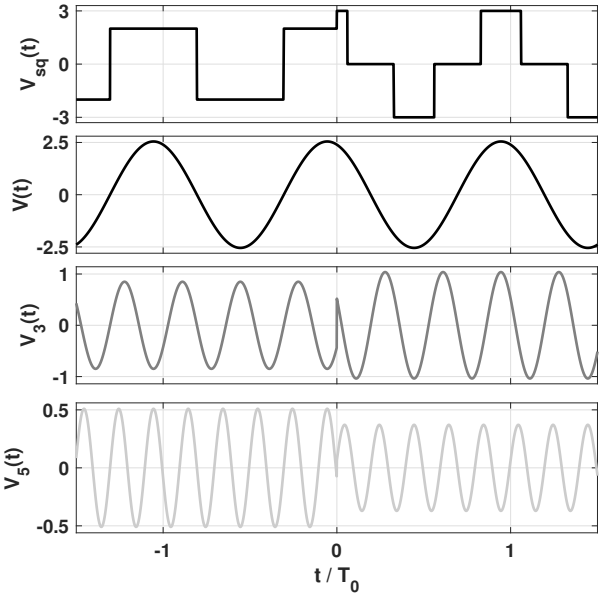

Fig. 5. Time-domain representation of an amplitude transition in multilevel outphasing with discontinuities in harmonics. The sinusoidal waveforms of the fundamental, 3rd and 5th harmonics are also depicted.

Therefore, performing amplitude transitions in multilevel outphasing corrupts the time-domain signal by causing discontinuities in the harmonic waveforms. As a consequence, the harmonics spread across the spectrum in frequency domain, as shown in Fig. 6, and set a limit on the achievable linearity of the transmitter. As wider modulation bandwidth generates larger and more rapid changes in signal envelope, signals with wider bandwidth will have more amplitude transitions and thus have a more negative impact on linearity.

B. Pulse Swallowing Caused by Amplitude Transitions

Multilevel operation increases the probability of narrow pulses in the SH-PM as the outphasing angle $\theta_{MO}(t)$ has large jumps when discrete amplitude transitions occur. $\theta_{MO}(t)$ can change abruptly by values up to $\pi/3$ as defined by (23). Pulse swallowing in the presence of an increasing amplitude transition with the SH-PM is demonstrated in Fig. 7(a). A narrow pulse is generated in the SM-PA that drives the signal

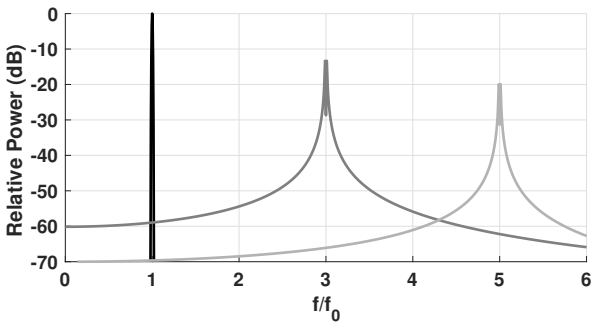

Fig. 6. Spectrum of an amplitude level transition that has discontinuities in harmonics.

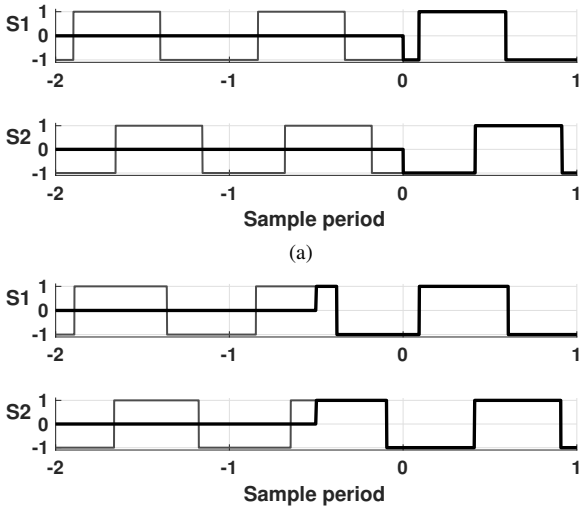

Fig. 7. Origin of narrow pulses in individual PA outputs in multilevel outphasing with (a) the SH-PM and (b) the DIPM. The waveforms present ideal signals without pulse swallowing, where black lines depict PA pairs that are turned on.

S_1 when it is turned on. As a consequence, the generated narrow pulses are swallowed within the SM-PA and distort the combined RF signal.

The DIPM by design does not generate narrow pulses even if the outphasing angle $\theta_{MO}(t)$ changes rapidly, as the minimum pulse width of the modulated signal is defined by $T_s/4$ [29]. However, a multilevel outphasing transmitter that utilizes the DIPM may produce narrow pulses when PAs are turned on or off, as is demonstrated in Fig. 7(b). Narrow pulses can be generated as the amplitude transition occurs at a fixed position during the sample period, which may be close to the transition of the phase-modulated signal.

C. Phase Interpolation and Amplitude Transitions

An additional source of distortion is caused by the phase interpolation in the DIPM when combined with instantaneous amplitude transitions of multilevel outphasing. The phase interpolation error is depicted in Fig. 8(a) with vector representations and in Fig. 8(b) with continuous envelope waveforms of the SH-PM and the DIPM. The amplitude transitions of $A_{MO}(t)$ are instantaneous, while the phase interpolation in

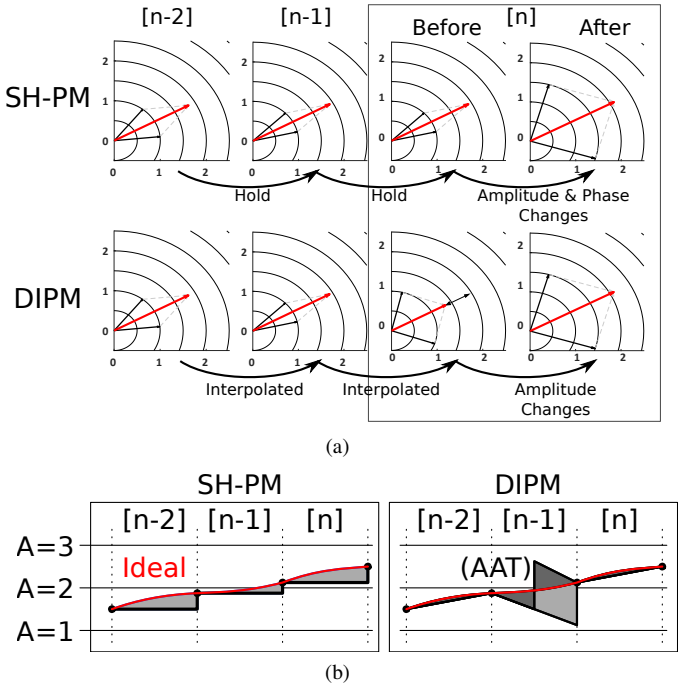

Fig. 8. Illustration of how the DIPM incorrectly interpolates the envelope near amplitude transitions. (a) Vector representation of an amplitude transition with the SH-PM and the DIPM. (b) Corresponding envelope waveforms.

$\rho_{int}[n,k]$ of (14) is performed between two sample periods. As a consequence, during the period preceeding the transition, the DIPM interpolates the significant difference in the outphasing angle $\theta(t)$. The premature interpolation generates error in the envelope up to one discrete amplitude level, as is shown in Fig. 8(b). As the error, positive or negative, is accumulated during the period, the magnitude of the error can be decreased by advancing the amplitude transition by half a sample period $(1/(2F_s))$. The advanced amplitude transition (AAT) is also visible in Fig. 7(b), which depicts time-domain signals. It should be noted that the interpolation error only occurs during sample periods with amplitude transitions. On the other hand, the SH-PM accumulates error due to sample-and-hold each sample period, which is also depicted in Fig. 8(b).

D. Summary

In conclusion, we state that multilevel outphasing with the SH-PM distorts the signal due to harmonic discontinuities and pulse swallowing. By utilizing the DIPM, the severity of pulse swallowing decreases. However, the DIPM incorrectly interpolates the envelope near amplitude transitions, and fails to achieve better ACLR than the SH-PM.

Fig. 9 shows the spectra of multilevel outphasing (MO) with the SH-PM and the DIPM, illustrating that the ACLR is limited regardless of the phase modulator architecture. Multilevel outphasing with four amplitude levels achieves at best only -54 dBc ACLR, which is a 7 dB degradation compared to single level outphasing that achieves -61 dBc, as was illustrated in Fig. 3. Furthermore, the reference ACLR with SH-PM degrades by an additional 6 dB when pulse swallowing is taken into account.

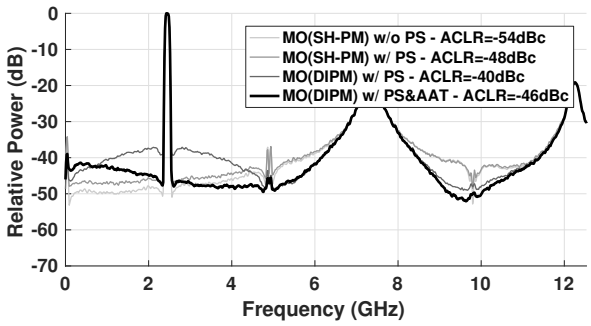

Fig. 9. Spectrum of 4-level multilevel outphasing (MO) utilizing the SH-PM and the DIPM, with and without pulse swallowing (PS). Transmitter linearity with the DIPM can be improved by advancing the amplitude transition (AAT) by half of a sample period.

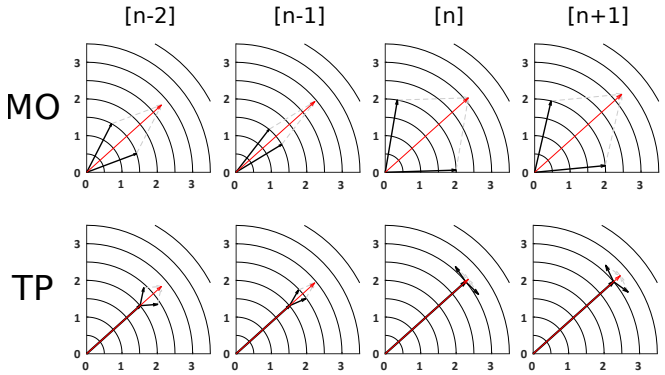

Fig. 10. Vector representation of multilevel outphasing (MO) and tri-phasing (TP) near an amplitude transition.

In order to improve the multilevel transmitter linearity, the signal composition must be performed in a way that the signal waveform does not have discontinuities. Furthermore, the interpolation of the DIPM should not distort the signal near amplitude transitions. This will be addressed next, in the form of a new tri-phasing transmitter concept.

IV. Proposed Tri-Phasing Concept

In order to address the signal degradation demonstrated with multilevel outphasing in the previous section, we propose a new multilevel transmitter architecture that does not produce narrow pulses nor discontinuities in the signal waveform near discrete amplitude transitions, and therefore can achieve high linearity. We begin by describing the signal composition and general operation principle of tri-phasing modulation. We then proceed to describe the proposed implementation that enables tri-phasing in modern CMOS transmitters. We then compare tri-phasing against multilevel outphasing and then conclude this section by describing the necessary changes that are required in the DIPM DSP for tri-phasing.

A. Signal Composition

As was demonstrated in Section III, the multilevel outphasing transmitter has discontinuities in its waveform that originate from discrete amplitude transitions. The discontinuities distort the signal and limit the achievable ACLR of the transmitter. Therefore, the tri-phasing architecture is designed to enable continuous amplitude transitions in the combined output waveform, while simultaneously solving pulse swallowing in individual signals. The signal composition is as follows:

$$V(t) = \frac{1}{2A_{max}} \left(2 \cdot A_{TP}(t) S_0(t) + S_1(t) + S_2(t)\right) \quad (24)$$

$$S_0(t) = \cos(\omega_c t + \phi(t)) \quad (25)$$

$$S_1(t) = \cos(\omega_c t + \phi(t) + \theta_{TP}(t)) \quad (26)$$

$$S_2(t) = \cos(\omega_c t + \phi(t) - \theta_{TP}(t)), \quad (27)$$

where the amplitude level $A_{TP}(t)$ and the outphasing angle $\theta_{TP}(t)$ are defined as

$$A_{TP}(t) = A_{MO}(t) - 1 \quad (28)$$

$$\theta_{TP}(t) = \arccos(r(t)A_{max} - A_{TP}(t)). \quad (29)$$

Thus, the polar modulator signal $S_0(t)$ is amplified by discrete amplitude levels that are defined by $A_{TP}(t)$, which provides coarse amplitude resolution of the envelope $r(t)$. Fine amplitude resolution between the discrete amplitude levels is provided by the outphasing modulators S_1 and S_2. Therefore, tri-phasing can be considered a hybrid between polar and outphasing. The operation of tri-phasing is compared to the operation of multilevel outphasing in Fig. 10, where the differences in signal compositions are depicted with vectors.

B. Continuous Amplitude Transitions

We can identify the properties that enable continuous amplitude transitions in the tri-phasing transmitter as:

- The discrete amplitude level $A_{TP}(t)$ does not affect the phase of the signal $S_0(t)$ that it interacts with.
- The amplitude transition is synchronized to the edges of the signal $S_0(t)$, which guarantees that the following PA unit outputs do not generate narrow pulses whether they are turned on or off.
- In order to make amplitude transitions invisible in $V(t)$, the phases of $S_1(t)$ and $S_2(t)$ are instantaneously shifted to compensate for the instantaneous change in the amplitude of $2 \cdot A_{TP}(t)S_0(t)$.
- By utilizing the DIPM, the instantaneous phase shifts can be performed in digital domain by re-defining the toggling instances of $S_1(t)$ and $S_2(t)$. This approach avoids the need for further distortion-prone analog signal processing.

As an example, we can consider the waveforms shown in Fig. 11, which depict an increasing amplitude transition with tri-phasing (TP) and multilevel outphasing (MO). The tri-phasing signals $S_0(t)$, $S_1(t)$ and $S_2(t)$ are also shown independently. The amplitude transition is marked with a dotted grey line, and it occurs as $S_0(t)$ toggles. As a consequence, a new PA unit is turned on, which is presented by the black line

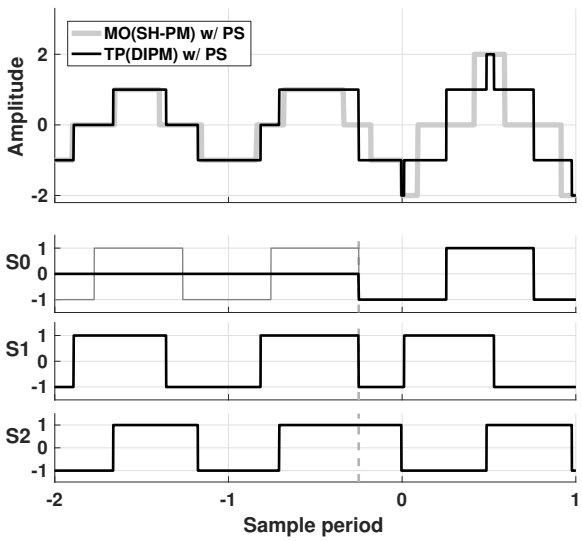

Fig. 11. Time-domain illustration of multilevel outphasing (MO) and tri-phasing (TP) near an amplitude transition. Waveforms of the three phase-modulated signals in tri-phasing are also presented separately. Before the amplitude transition at the dotted grey line, the outphasing modulators S_1 and S_2 are in phase, and after the transition they are out of phase.

in $S_0(t)$ waveform. As the amplitude transition is synchronized to the edge of $S_0(t)$, narrow pulses can be avoided in PA units driving $S_0(t)$, which contributes most to the complete signal vector $V(t)$.

At the time of the transition at the dotted grey line, the phase difference of signals $S_1(t)$ and $S_2(t)$ approaches zero. Simultaneously as the additional PA unit pair is turned on, the increasing amplitude is compensated by the instantaneous phase shift of $S_1(t) + S_2(t)$, as $\theta_{TP}(t)$ jumps from 0 to $\pi/2$. As a consequence, the amplitude transition becomes invisible in the time-domain waveform $V(t)$, allowing the envelope to increase without abrupt changes.

We propose that the DIPM can be used to implement the tri-phasing transmitter, as it calculates the location of phase modulator toggling instances within the sample period in digital domain. This information can be passed between phase modulators to accurately realize the instantaneous phase shift. Thus, we can precisely calculate the moment when the polar modulator $S_0(t)$ toggles in digital domain, which in turn defines the amplitude transition instant and the instantenous phase shift in the outphasing modulators. The details of the phase modulator operation in tri-phasing are described in Section IV-E.

C. Implementation

The block diagram of the proposed tri-phasing transmitter is presented in Fig. 12. As described, the tri-phasing transmitter requires three digital interpolating phase modulators (DIPMs): two outphasing modulators and one polar modulator whose output is driven to multiple PAs as defined by A_{TP}. The synchronization between the polar modulator transitions to the amplitude data of $A_{TP}[n]$ can be acquired from the polar modulator zero crossings by utilizing a first-in-first-out (FIFO)

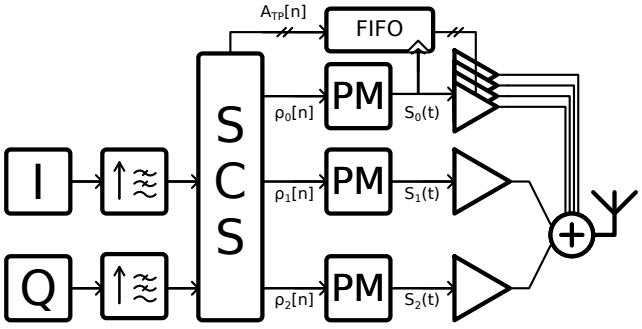

Fig. 12. Block diagram of the proposed tri-phasing transmitter.

buffer sensitive to rising and falling transitions. The $A_{TP}[n]$ data can be driven to the FIFO with the number of transitions and amplitude values at each sample period, and fetched at polar modulator transitions. With the proposed tri-phasing architecture, the DIPM core as presented in [29] does not require any modifications as all required modifications are part of the DIPM solver DSP, or the SCS.

Although the tri-phasing architecture is more complex than conventional multilevel outphasing, the increased complexity can be justified when substantial improvement to the transmitter linearity is required, as will be demonstrated in Section V.

1) Hardware Cost: The tri-phasing architecture can improve the linearity over multilevel outphasing, but the improved linearity comes with additional cost of increased power consumption and area in the low-power circuits in the transmitter chain. The cost of improving transmitter linearity is already partly included in the requirements for high sample rate and high resolution in the phase modulator. When compared against multilevel outphasing, the additional hardware cost comes mainly due to the third phase modulator. Synchronizing the amplitude transitions and the phase modulated signals with the DIPM architecture further increases this cost. However, detailed power consumption or area estimates for the low-power front end for the transmitter are not essential to the concept, as most of the transmitter chain power is ultimately consumed in the PAs. This is especially the case in basestation applications. The tri-phasing architecture therefore enables high efficiency with multilevel SM-PAs, without compromising transmitter linearity and wide signal bandwidth. Thus, higher power consumption in the low-power circuits can be justified if high efficiency and linearity can be provided for the complete transmitter chain.

2) Suitable PA and Power Combiner Architectures: The high power circuits in tri-phasing support similar architectures as multilevel outphasing, where the amplitude level is scaled instantaneously. The signal composition and system-level model presented in this paper is designed for parallel SM-PA units that are turned on or off, as presented in [23]. However, the tri-phasing architecture can also be adapted to SM-PAs with amplitude level control by means of discrete supply levels [22], [26].

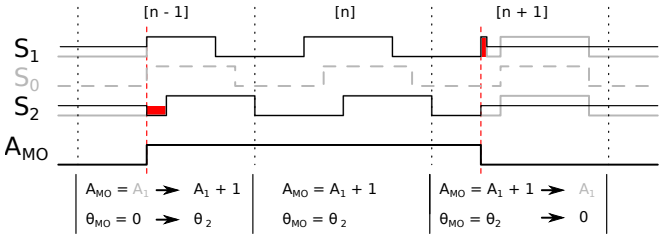

Fig. 13. An illustration of the origin of narrow pulses in a multilevel outphasing transmitter, if the amplitude transitions are performed at the first phase modulator transition within the sample period. The polar modulator S_0 is included to clarify the phase differences between S_1 and S_2.

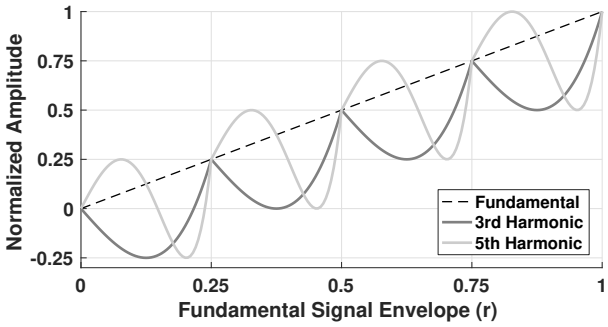

Fig. 14. Normalized amplitudes of the third and fifth harmonic components as a function of the fundamental amplitude in tri-phasing.

D. Comparison to Multilevel Outphasing

1) Amplitude Transitions and Narrow Pulses: In multilevel outphasing, narrow pulses cannot be avoided even if amplitude transitions are synchronized with the phase-modulated signal. This is due to the fact that phase jumps of θ_{MO} and amplitude transitions of A_{MO} are associated with the same phase-modulated signals $S_1(t)$ and $S_2(t)$, which make narrow pulses unavoidable near amplitude transitions. For example, we can consider a design where the amplitude transition is performed at the first phase modulator transition during the sample period. Such behavior is illustrated in Fig. 13, where increasing and decreasing transitions are shown to generate narrow pulses. As depicted in the left side of the figure at an increasing transition, the waveform S_2 may generate a narrow pulse (red box) in the PA that is turned on (black line). θ_2 defines the pulse width generated in $S_2(t)$, which can be narrow enough not to be reproducible. A decreasing amplitude transition always requires a narrow pulse in $S_1(t)$, as the rising edge is required for initiating the amplitude transition. However, after the transition θ_{MO} is zero and $S_1(t)$ should instantaneously be low again.

2) Behavior of Harmonics at Amplitude Transitions: In tri-phasing, the outphasing angle instantaneously shifts between 0 and $\pi/2$ at every amplitude level transition. The behavior of the harmonics can be described in tri-phasing by utilizing the same approach that was applied in Section III-A. By considering the signal composition in tri-phasing, the amplitude of the nth harmonic in the output signal can be expressed as

$$\begin{aligned} A(n,r) &= \frac{1}{A_{max}}\frac{4}{n\pi}\left(A_{TP}(r) + \cos(n\theta(r))\right) \\ &= A_0(n)\left(A_{TP}(r) + \cos(n\theta(r))\right). \end{aligned} \tag{30}$$

In a scenario before an increasing amplitude transition where the discrete amplitude level is A_1 and the outphasing angle is 0, it can be shown that for any harmonic n that the harmonic amplitude is

$$A = A_0(A_1 + \cos(0)) = A_0(A_1 + 1). \tag{31}$$

After the transition to amplitude level $A_1 + 1$ and outphasing angle $\pi/2$, the harmonic amplitude becomes

$$A = A_0\left(A_1 + 1 + \cos\left(n\frac{\pi}{2}\right)\right) = A_0(A_1 + 1). \tag{32}$$

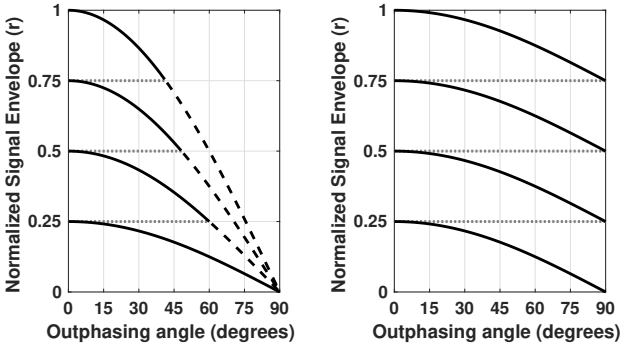

Fig. 15. Signal envelope magnitude as a function of the outphasing angle in (a) multilevel outphasing and (b) tri-phasing.

Thus, the harmonic amplitude remains the same on both sides of the transition, demonstrating that in tri-phasing odd harmonic component amplitudes are always continuous during amplitude transitions, unlike in multilevel outphasing. This is illustrated in Fig. 14, depicting the third and fifth harmonics as a function of the fundamental component amplitude.

3) Output Amplitude Behavior: The output envelope is depicted as a function of the outphasing angle for multilevel outphasing in Fig. 15(a), and for tri-phasing in Fig. 15(b). In multilevel outphasing some of the outphasing angle range is redundant, except at the lowest amplitude level, since an equal output amplitude can be achieved with lower amplitude levels. These parts are shown as dashed lines. In contrast, this redundancy does not exist in tri-phasing as the entire outphasing angle range is used at all levels, which effectively increases the output amplitude resolution.

4) Efficiency: The multilevel efficiency improvement with parallel SM-PAs is dependent on the PA class as well as the power combiner architecture. Here we consider an ideal power combiner with class-D PAs, and assume that disabled PAs do not consume any power. Hence, the total efficiency can be calculated as as a function of output power P_{out} and DC power consumption P_{dc} as

$$\eta_{tx}(r) = \frac{P_{out}}{P_{dc}} = \frac{r^2}{r^2 + A_{MO}(r)\cdot P_{loss}}, \tag{33}$$

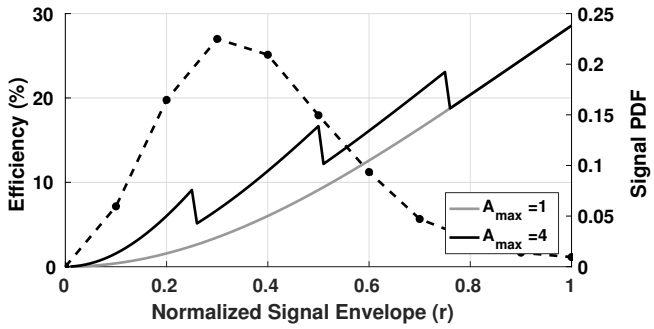

Fig. 16. Efficiency of class-D PAs in single or multilevel operation as a function of signal envelope, including the envelope PDF of a 100 MHz signal with 8 dB PAPR.

which yields efficiency curves as shown in Fig. 16 with 1 and 4 discrete amplitude levels. Each enabled PA has an intrinsic constant power loss factor of $P_{loss} = 2.5$, leading to results that match closely to measurement results obtained in [23]. Since the number of active PA pairs at a specific output power level is the same between multilevel outphasing and tri-phasing, the PA efficiency as a function of output power is also equal in both architectures. The probability density function (PDF) of a 100 MHz aggregated 64-QAM OFDM signal envelope with 8 dB PAPR is also included to highlight the achievable efficiency improvement in power back off. Modulation efficiency of the 100 MHz signal can be estimated from the signal PDF and efficiency curves in Fig. 16, yielding approximately 5.6% for outphasing and 9.4% for multilevel architectures. Multilevel operation thus improves the considered PA configuration efficiency by 68%.

E. Tri-Phasing DSP with the DIPM

The tri-phasing DSP performs data and block-dependent operations during sample periods to achieve continuous amplitude transitions. In order to demonstrate that the concept is feasible, the DSP operation is described in detail.

In normal operation, the three phase modulators can perform one step linear interpolation as described in (14) and locate the zero crossings based on (16). If the sample period has an amplitude transition that is indicated by a change in $A_{TP}[n]$, the tri-phasing DSP first solves the optimum polar modulator zero crossing. The polar crossing toggles the amplitude transition, and serves as a reference for the outphasing modulators to perform two step interpolation that generates the instantaneous $\pi/2$ phase jump.

1) Locating the Polar Modulator Zero Crossing: The DIPM responsible for the polar phase $\rho_0[n]$ can estimate the polar crossings with a single interpolation per sample period as shown in (16). The potential zero crossing locations are denoted by X_i. If several crossings exist, the crossing located nearest to the middle of the sample period $X_A[n]$ is chosen to be used as a reference for the amplitude transition. When $X_A[n]$ is close to the middle of the period, the envelope interpolation is balanced between the two interpolation stages.

The lower the generated carrier frequency is in the DIPM, the more infrequent the zero crossings become. For example in the case of $f_c = F_s/4$, a crossing occurs on average only once in two consecutive sample periods. Thus, there can be a situation where the discrete amplitude level should change as indicated by $A_{TP}[n] \neq A_{TP}[n-1]$, but the polar modulator does not have any zero crossing $X_A[n]$ during that period. If such an event occurs, the tri-phasing DSP delays the amplitude transition to the following period and waits for the next $X_A[n]$. In addition to delaying the amplitude transition, the outphasing angle is set to the boundary value with either minimum or maximum amplitude, and waits for the amplitude transition. As a consequence, the signal becomes somewhat distorted as the envelope remains static until a zero crossing is found. However, this approach guarantees that narrow pulses are not generated and thus any unpredictable behavior can be avoided.

2) Outphasing Modulator Interpolation Near Amplitude Transitions: If a value for $X_A[n]$ is found, then the outphasing modulators perform the interpolation in two stages to account for the $\pi/2$ phase jump. The phase values before and after the phase jump are dependent on the direction of the amplitude transition and are either equal to the polar modulator or with $\pm\pi/2$ phase offset. In the case of an increasing amplitude level the outphasing phases are interpolated to be in-phase with the polar modulator right before the transition, thus providing maximum amplitude, and shifted out-of-phase after the transition, providing zero amplitude. The order of the phases is reversed when the amplitude level decreases.

The two interpolation stages are defined as

$$\rho_{i,int1}[n,k] = \rho_i[n-1] + \frac{k}{X_A[n]} \cdot \Delta\rho_{i,end1}[n], \quad k \in \{1,2,3,...,X_A[n]\} \tag{34}$$

$$\rho_{i,int2}[n,h] = \rho_{i,jump}[n] + \frac{h}{K_x[n]} \cdot \Delta\rho_{i,end2}[n], \quad h \in \{1,2,3,...,K_x[n]\}, \quad K_x[n] = K - X_A[n], \tag{35}$$

where the intermediate unwrapped phase values are

$$\Delta\rho_{i,end1}[n] = \rho_{0,int}\left(n, X_A[n]\right) - \rho_i[n-1] \tag{36}$$

$$\rho_{1,jump}[n] = \rho_{0,int}\left(n, X_A[n]\right) + \frac{\pi}{2} \tag{37}$$

$$\rho_{2,jump}[n] = \rho_{0,int}\left(n, X_A[n]\right) - \frac{\pi}{2} \tag{38}$$

$$\Delta\rho_{i,end2}[n] = \rho_i[n] - \rho_{i,jump}[n], \tag{39}$$

where $\rho_{i,jump}[n]$ is defined by the $\pm\pi/2$ phase jump from the polar zero crossing $X_A[n]$. The tri-phasing interpolation scheme is illustrated graphically in Fig. 17 for the polar modulator ρ_0 and outphasing modulators ρ_1 and ρ_2 with two-stage phase interpolation defined by (34) and (35).

A consequence of the instantaneous $+\pi/2$ phase jump is that the pulse width of one phase modulator decreases. Due to hardware limitations, each of the four DTCs within the DIPM can only process a single sign toggling event per sample period. This relates to a maximum allowable phase increment of π for one fourth of the sample period as

$$\Delta\rho_{max} = \frac{\alpha + \Delta\phi[n] \pm \Delta\rho[n]}{4} + \frac{\pi}{2} \leq \pi, \tag{40}$$

which is dependent on α as well as the change in modulating phase $\Delta\Phi[n]$. As the modulating phase difference is typically

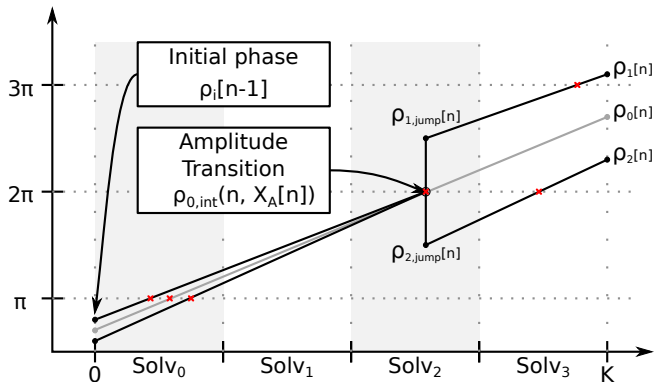

Fig. 17. A graphical illustration of the two-stage phase interpolation required by the three different phase modulators in tri-phasing. The locations of the zero crossings are indicated with red crosses.

TABLE I
SIMULATION PARAMETERS.

Signal Bandwidth	100 MHz
Modulation	OFDM (64-QAM)
Signal PAPR	8 dB
Sample Rate	2.46 GHz
Carrier Frequency	2.46 GHz
Phase Resolution	10 bits
Amplitude Resolution	2 bits
Pulse-Swallowing Threshold	80 ps

a small positive or negative value, it is simpler to investigate the behavior as a function of the carrier frequency f_c. With $f_c = F_s$ the equation becomes

$$\Delta\rho_{max} = \frac{2\pi + \Delta\phi[n] \pm \Delta\rho[n]}{4} + \frac{\pi}{2} \leq \pi, \qquad (41)$$

which relates as a requirement to the modulating phase as

$$\Delta\phi[n] \pm \Delta\rho[n] \leq 0. \qquad (42)$$

If this statement does not hold and $X_A[n]$ is located in one of the first samples of the solver, two crossings with less than a $\pi/2$ difference may occur within a single solver. As a single DTC in the DIPM core can only generate one event that toggles the sign of the phase modulator, the other event would thus be discarded and the phase of the modulator becomes shifted by an offset equal to π. However, the DSP can be implemented in a way that these events are detected and handled appropriately. One approach is that the second event is transferred to the first value of the following DTC. This leads only to minor distortion assuming that $\Delta\Phi[n]$ remains small. An alleviating factor for this drawback is that the largest $\Delta\phi[n]$ occurs when the polar vector length $r(t)$ is small and near the origin [6], and thus far from amplitude transitions.

V. PERFORMANCE EVALUATION BY SIMULATIONS

A. Transmitter Characteristics

The simulations in this paper were performed with the parameters defined in the Table I, unless stated otherwise. The chosen 100 MHz baseband signal bandwidth (BW) is the widest supported signal bandwidth for 5G networks operating at the lower frequency range (FR1) [1]. As our existing signal generation environment does not yet support 5G compliant signal generation, we utilize five aggregated 20 MHz 64-QAM LTE downlink carriers to form the 100 MHz test signal. The original baseband signal has a peak to average power ratio (PAPR) of 12.6 dB, but PAPR reduction has been used to achieve 8 dB PAPR. In order to maximize the transmitter performance, the signal component separator and the phase modulator are clocked at the carrier frequency, such that $F_s = f_c = 2.46\,\text{GHz}$. The phase modulator resolution is 10 bits, and thus the sample period is quantized into $K = 2^{10} = 1024$ steps with a delay resolution of approximately 400 fs, which has been shown to be feasible in [32] with accurate calibration of a digitally controlled delay line. The transmitter multilevel amplitude resolution is 2 bits, corresponding to $A_{max} = 4$. Pulse swallowing is enabled and the threshold value is set to 80 ps, corresponding to approximately one fifth of the carrier period when $F_s = f_c$.

B. ACLR and EVM performance

Fig. 18 presents simulated close-up spectra of a 100 MHz aggregated LTE downlink signal with different transmitter architectures. Fig. 18(a) shows the spectrum of the outphasing transmitter utilizing the DIPM, which is shown to be capable of an ACLR of -61 dBc. In Fig. 18(b), the spectrum of a multilevel outphasing transmitter utilizing the SH-PM achieves -48 dBc ACLR, while the DIPM in Fig. 18(c) achieves only -46 dBc. The tri-phasing transmitter spectrum is shown in Fig. 18(d), achieving an ACLR of -58 dBc and demonstrating an ACLR improvement of 10 dB compared to the multilevel outphasing transmitter. Thus, the best ACLR of -61 dBc is achieved with outphasing and the DIPM, and the tri-phasing transmitter is capable of nearly the same ACLR with -58 dBc, while significantly improving the efficiency over outphasing, as was depicted in Fig. 16.

The error vector magnitude (EVM) is compared between the architectures in Fig. 19 without utilizing PAPR reduction. PAPR reduction to 8 dB preserves the ACLR of the signal, but degrades the baseband signal EVM to approximately 4%, thus making direct EVM comparison unfeasible. The single-level outphasing (SO) and tri-phasing (TP) architectures achieve down to 0.2% EVM, whereas the multilevel outphasing (MO) architecture is limited to approximately 0.5% EVM regardless of the utilized phase modulator. However, all of the EVM results are still well below the LTE EVM specification of 8% with 64-QAM, and also meet the 256-QAM EVM specification of 3.5%.

Fig. 20 shows the wide-span spectra with each transmitter architecture. The figure demonstrates that the architecture choise also has a significant impact on the achievable out-of-band noise level. Tri-phasing can achieve nearly as good performance as outphasing, while the noise floor remains at a much higher level in multilevel outphasing regardless of the phase modulator that is used.

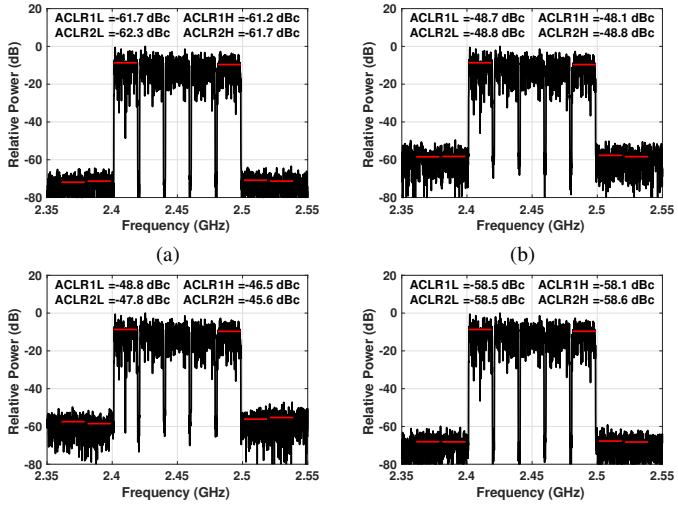

Fig. 18. Simulated ACLR of (a) outphasing utilizing the DIPM, multilevel outphasing utilizing the (b) SH-PM or (c) the DIPM, and (d) tri-phasing with the DIPM.

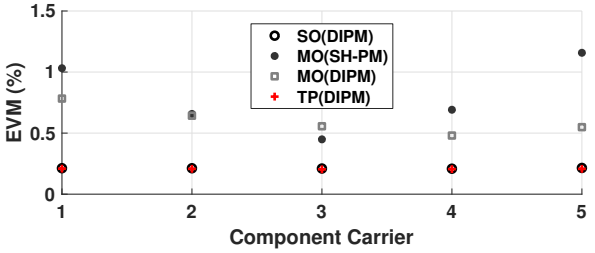

Fig. 19. EVM comparison between transmitter architectures.

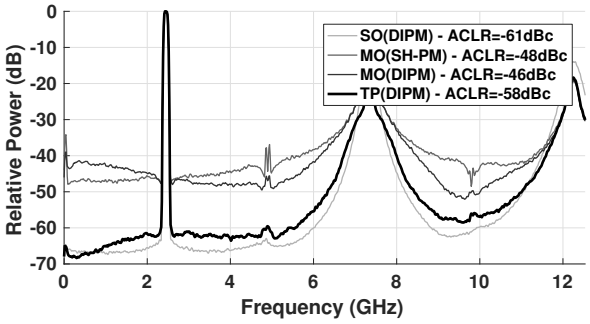

Fig. 20. Wide-span spectra of the transmitter architectures that are compared in this paper.

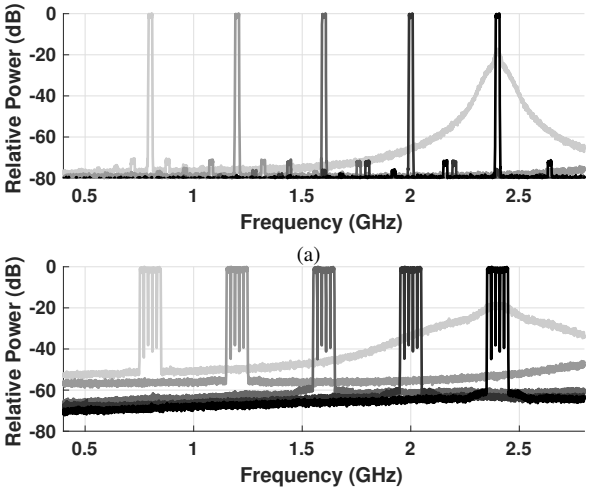

Fig. 21. Digital carrier generation demonstrated with tri-phasing by utilizing the DIPM at 2.46 GHz sample rate with (a) 20 MHz and (b) 100 MHz signals.

C. Digital Carrier Generation

Tri-phasing utilizes the DIPM in its core, which enables digital carrier generation at an arbitrary frequency below the phase modulator sample rate [29]. Based on (13), the transmitter carrier frequency can be altered by only changing the value of the digital variable α. The carrier frequency can thus be altered without changing the phase modulator sample rate, enabling transmitter operation without external frequency synthesizers.

Digital carrier generation is demonstrated by sweeping the carrier frequency between 0.8–2.4 GHz in 400 MHz steps. The spectra with a 20 MHz LTE downlink signal are shown in Fig. 21(a), and with a 100 MHz aggregated LTE signal in Fig. 21(b). The visible ACLR degradation at carrier frequencies lower than $F_s/2$ with the 100 MHz signal can be explained by missing polar modulator zero crossings, which constrain the envelope of a rapidly varying signal for one or several sample periods. The longer the envelope is constrained, the larger the distortion caused by this operation becomes. In the sub-gigahertz range where signal bandwidths are small and the ACLR degradation is dominated by the constrained envelope, the sample rate of the transmitter can be divided by an integer factor in order to maintain linearity and decrease power consumption.

D. Effect of Amplitude and Phase Resolution

The ACLR of tri-phasing is also compared against multilevel outphasing as a function of amplitude and phase resolution with 20 MHz and 100 MHz LTE signals. Fig. 22(a) shows the ACLR as a function of amplitude resolution. Here, 0 bit resolution corresponds to outphasing, and 4 bit resolution corresponds to $2^4 = 16$ discrete amplitude levels. The ACLR degradation of tri-phasing with higher amplitude resolution is explainable by amplitude transitions over multiple amplitude levels. Changing the amplitude multiple levels at one instance breaks the envelope interpolation and makes it noncontinuous. Thus, tri-phasing is capable of achieving the lowest distortion when operated with only a few discrete amplitude levels.

Fig. 22(b) depicts the ACLR as a function of the phase resolution. The figure demonstrates how tri-phasing is capable of nearly five times larger bandwidth than multilevel outphasing with equal ACLR. On the other hand, increasing the phase resolution above 8 bits with a 100 MHz signal shows only minor ACLR improvement, suggesting that the ACLR is limited by bandwidth expansion. Thus, a higher sample rate would be required to further improve the ACLR.

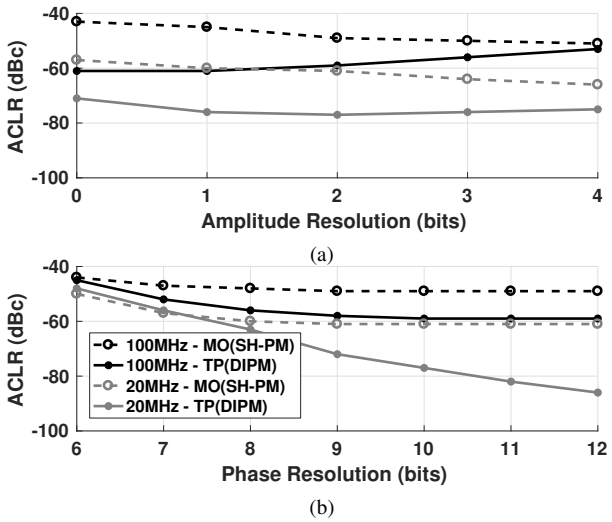

Fig. 22. ACLR of multilevel outphasing (MO) compared to tri-phasing (TP) as a function of: (a) Amplitude resolution with 20MHz and 100MHz signal bandwidths, with phase resolution of 10 bits. (b) Phase resolution, with amplitude resolution of 2 bits.

TABLE II
COMPARISON BETWEEN TRANSMITTER ARCHITECTURES THAT UTILIZE THE DIPM.

	SO	MO	TP
TX-FE Power Consumption (mW)	$1x$	$\sim 1x$	$\sim 1.5x$
Relative Complexity	Low	Medium	High
Linearity (ACLR, dBc)	-61.2	-46.5	-58.1
PA Efficiency	$1x$	$1.68x$	$1.68x$

E. System-Level Comparison

The transmitter architectures discussed in this paper are compared in Table II, with the assumption that the DIPM is utilized. The transmitter low-power front end (TX-FE) power and active area consumption are dominated by the number of PMs, although some additional circuitry is required in multilevel outphasing and tri-phasing. The relative complexity between the architectures can also be coarsely identified. Outphasing (SO) is the simplest architecture that we have considered, whereas multilevel outphasing (MO) and tri-phasing (TP) require either a more complex power combiner or a discrete supply modulator to enable multilevel operation. Furthermore, tri-phasing requires a third phase modulator and more complex DSP than the other two architectures, thus making it the most complex architecture. The transmitter linearity is expressed in terms of achievable ACLR of an aggregated 100 MHz LTE signal with 10-bit phase resolution. The PA efficiency numbers have been extracted from Fig. 16, presenting values with class-D PAs and ideal power combining.

To summarize, the tri-phasing architecture requires more complex design and higher power consumption in the TX-FE. These drawbacks enable improving the PA efficiency by 68% when compared to outphasing, with minor degradation in ACLR. Alternatively, tri-phasing can improve the ACLR of a 100 MHz aggregated LTE signal by over 10 dB when compared to multilevel outphasing.

VI. CONCLUSION

In this paper, we have presented a new transmitter architecture that aims to improve the linearity and bandwidth of efficient multilevel transmitters. The tri-phasing transmitter is capable of eliminating sources of distortion such as harmonic spreading and pulse swallowing, which are demonstrated to be inherent in the multilevel outphasing architecture. The tri-phasing transmitter requires an additional phase modulator and more evolved digital signal processing to improve the linearity over multilevel outphasing.

In addition to architectural modifications, the tri-phasing transmitter utilizes the digital interpolating phase modulator in its core, enabling superior sampling image suppression and distortion free time-domain waveform generation. Furthermore, the phase modulator enables digital carrier generation to frequencies below the phase modulator sample rate, which removes the need for external frequency synthesizers. The digital interpolating phase modulator also plays a key role in enabling continuous amplitude transitions for the tri-phasing transmitter. The amplitude transitions are performed simultaneously when the polar modulator changes its state during the sampling period. The time-domain signal processing required by tri-phasing is performed completely with DSP, which pushes the boundary of the transmitter entity to the digital domain and reduces the complexity of the analog RF front-end.

The tri-phasing transmitter is capable of achieving an ACLR of -58dBc with a 100 MHz aggregated LTE downlink signal, while the multilevel outphasing transmitter is limited to -48dBc ACLR when simulated with equal transmitter parameters, including sample rate of 2.46 GHz, 10 bit phase resolution and 4 discrete amplitude levels. Tri-phasing is thus capable of significant ACLR improvement over the multilevel outphasing architecture by enabling continuous amplitude transitions with discrete amplitude levels.

REFERENCES

[1] *Base Station (BS) radio transmission and reception*, 3GPP Std. TS 38.104, Rev. 15.0.0, Jan. 2017.
[2] J. G. Andrews *et al.*, "What will 5G be?" *IEEE Journal on Selected Areas in Communications*, vol. 32, no. 6, pp. 1065–1082, June 2014.
[3] F. Boccardi, R. W. Heath, A. Lozano, T. L. Marzetta, and P. Popovski, "Five disruptive technology directions for 5g," *IEEE Communications Magazine*, vol. 52, no. 2, pp. 74–80, February 2014.
[4] R. Shrestha, R. van der Zee, A. de Graauw, and B. Nauta, "A wideband supply modulator for 20 MHz RF bandwidth polar PAs in 65 nm CMOS," *IEEE J. Solid-State Circuits*, vol. 44, no. 4, pp. 1272–1280, April 2009.
[5] P. Y. Wu and P. K. T. Mok, "A two-phase switching hybrid supply modulator for RF power amplifiers with 9% efficiency improvement," *IEEE J. Solid-State Circuits*, vol. 45, no. 12, pp. 2543–2556, Dec 2010.
[6] J. Zhuang, K. Waheed, and R. Staszewski, "A technique to reduce phase/frequency modulation bandwidth in a polar RF transmitter," *IEEE Trans. Circuits Syst. I*, vol. 57, no. 8, pp. 2196–2207, Aug 2010.
[7] S.-M. Yoo, J. Walling, E. C. Woo, B. Jann, and D. Allstot, "A switched-capacitor RF power amplifier," *IEEE J. Solid-State Circuits*, vol. 46, no. 12, pp. 2977–2987, Dec 2011.
[8] K. F. Liang, H. S. Yang, C. W. Chang, and J. H. Chen, "A wideband pulse-modulated polar transmitter using envelope correction for LTE applications," *IEEE Trans. Microw. Theory Tech.*, vol. 63, no. 8, pp. 2603–2608, Aug 2015.
[9] S. Zheng and H. C. Luong, "A WCDMA/WLAN digital polar transmitter with low-noise ADPLL, wideband PM/AM modulator, and linearized PA," *IEEE J. Solid-State Circuits*, vol. 50, no. 7, pp. 1645–1656, July 2015.

[10] P. Madoglio *et al.*, "A 2.4GHz WLAN digital polar transmitter with synthesized digital-to-time converter in 14nm trigate/FinFET technology for IoT and wearable applications," in *IEEE Int. Solid-State Circuits Conf. Dig. Tech. Papers (ISSCC)*, San Francisco, CA, USA, Feb 2017, pp. 226–227.
[11] H. Chireix, "High power outphasing modulation," *Proc. IRE*, vol. 23, no. 11, pp. 1370–1392, Nov 1935.
[12] D. Cox, "Linear amplification with nonlinear components," *IEEE Trans. Commun.*, vol. 22, no. 12, pp. 1942–1945, Dec 1974.
[13] I. Hakala *et al.*, "A 2.14-GHz chireix outphasing transmitter," *IEEE Trans. Microw. Theory Tech.*, vol. 53, no. 6, pp. 2129–2138, June 2005.
[14] A. Ravi *et al.*, "A 2.5GHz delay-based wideband OFDM outphasing modulator in 45nm-LP CMOS," in *Symp. VLSI Circuits (VLSIC)*, Honolulu, HI, USA, June 2011, pp. 26–27.
[15] ——, "A 2.4-GHz 20–40-MHz channel WLAN digital outphasing transmitter utilizing a delay-based wideband phase modulator in 32-nm CMOS," *IEEE J. Solid-State Circuits*, vol. 47, no. 12, pp. 3184 –3196, dec. 2012.
[16] D. Calvillo-Cortes *et al.*, "A package-integrated chireix outphasing RF switch-mode high-power amplifier," *IEEE Trans. Microw. Theory Tech.*, vol. 61, no. 10, pp. 3721–3732, Oct 2013.
[17] G. Yahalom and J. L. Dawson, "A fast settling phase modulator for outphasing transmitters in 65-nm CMOS," *IEEE Trans. Microw. Theory Tech.*, vol. 62, no. 9, pp. 2048–2058, Sept 2014.
[18] M. Mehrjoo, S. Zihir, G. Rebeiz, and J. Buckwalter, "A 1.1-Gbit/s 10-GHz outphasing modulator with 23-dBm output power and 60-dB dynamic range in 45-nm CMOS SOI," *IEEE Trans. Microw. Theory Tech.*, vol. PP, no. 99, pp. 1–12, 2015.
[19] Y. Jung, J. Fritzin, M. Enqvist, and A. Alvandpour, "Least-squares phase predistortion of a +30 dbm Class-D outphasing RF PA in 65 nm CMOS," *IEEE Trans. Circuits Syst. I*, vol. 60, no. 7, pp. 1915–1928, July 2013.
[20] J. Laskar *et al.*, "Emerging multi-level architectures and unbalanced mismatch calibration technique for high-efficient and high-linear LINC systems," in *Circuits and Systems (ISCAS), Proceedings of 2010 IEEE International Symposium on*, Paris, France, May 2010, pp. 821–824.
[21] J. Hur, O. Lee, K. Kim, K. Lim, and J. Laskar, "Highly efficient uneven multi-level linc transmitter," *Electronics Letters*, vol. 45, no. 16, pp. 837–838, July 2009.
[22] P. Godoy, S. Chung, T. Barton, D. Perreault, and J. Dawson, "A 2.4-GHz, 27-dBm asymmetric multilevel outphasing power amplifier in 65-nm CMOS," *IEEE J. Solid-State Circuits*, vol. 47, no. 10, pp. 2372–2384, 2012.
[23] W. Tai *et al.*, "A transformer-combined 31.5 dBm outphasing power amplifier in 45 nm LP CMOS with dynamic power control for back-off power efficiency enhancement," *IEEE J. Solid-State Circuits*, vol. 47, no. 7, pp. 1646–1658, July 2012.
[24] A. Banerjee, L. Ding, and R. Hezar, "High efficiency multi-mode outphasing RF power amplifier in 45nm CMOS," in *ESSCIRC Conference 2015 - 41st European Solid-State Circuits Conference (ESSCIRC)*, Graz, Austria, Sept 2015, pp. 168–171.
[25] J. Hur *et al.*, "A multilevel class-D CMOS power amplifier for an outphasing transmitter with a nonisolated power combiner," *IEEE Trans. Circuits Syst. II*, vol. 63, no. 7, pp. 618–622, July 2016.
[26] C. T. Nghe *et al.*, "160 w peak highly linear multilevel outphasing transmitter," in *2016 46th European Microwave Conference (EuMC)*, London, UK, Oct 2016, pp. 1091–1094.
[27] Y. Tajima *et al.*, "Improved efficiency in outphasing power amplifier by mixing outphasing and amplitude modulation," in *2017 IEEE Topical Conference on RF/Microwave Power Amplifiers for Radio and Wireless Applications (PAWR)*, Phoenix, AZ, USA, Jan 2017, pp. 55–58.
[28] T. Cappello, T. W. Barton, C. Florian, M. Litchfield, and Z. Popovic, "Multilevel supply-modulated chireix outphasing with continuous input modulation," *IEEE Trans. Microw. Theory Tech.*, vol. PP, no. 99, pp. 1–13, 2017.
[29] J. Lemberg *et al.*, "Digital interpolating phase modulator for wideband outphasing transmitters," *IEEE Trans. Circuits Syst. I*, vol. 63, no. 5, pp. 705–715, May 2016.
[30] M. Kosunen *et al.*, "A 0.35–2.6 GHz multilevel outphasing transmitter with a digital interpolating phase modulator enabling up to 400 MHz instantaneous bandwidth," in *2017 IEEE International Solid-State Circuits Conference Digest of Technical Papers*, no. 13.5, San Francisco, CA, USA, 2017.
[31] D. Seebacher *et al.*, "Reduction of aliasing effects of RF PWM modulated signals by cross point estimation," *IEEE Trans. Circuits Syst. I*, vol. 61, no. 11, pp. 3184–3192, Nov 2014.
[32] C. Palattella, E. Klumperink, J. Ru, and B. Nauta, "A sensitive method to measure the integral nonlinearity of a digital-to-time converter based on phase modulation," *IEEE Trans. Circuits Syst. II*, vol. 62, no. 8, pp. 741–745, Aug 2015.

Jerry Lemberg (S'16) was born in Lohja, Finland, in 1986. He received his Master of Science degree in electrical engineering from Aalto University, Espoo, Finland, in 2013. He is currently working towards the Doctoral degree at Aalto University, Department of Electronics and Nanoengineering. His research interests include digital-intensive radio transmitters and high-speed digital-to-analog converters.

Mikko Martelius (S'16) was born in Laitila, Finland, in 1988. He received his B.Sc. and M.Sc. (with distinction) degrees in electrical engineering from Aalto University, Espoo, Finland, in 2012 and 2015, respectively. He is currently working towards the Doctoral degree at Aalto University, Department of Electronics and Nanoengineering. His research interests include switch-mode power amplifiers and digital-intensive transmitters.

Marko Kosunen (S'97-M'07) received his M.Sc, L.Sc and D.Sc (with honors) degrees from Helsinki University of Technology, Espoo, Finland, in 1998, 2001 and 2006, respectively. He is currently a Senior Researcher at Aalto University, Department of Electronics and Nanoengineering. His expertise is in implementation of the wireless transceiver DSP algorithms and communication circuits. He is currently working on implementations of cognitive radio spectrum sensors, digital intensive transceiver circuits and medical sensor electronics.

Enrico Roverato was born in Padua, Italy, in 1988. He received the B.Sc. degree *cum laude* in information engineering from the University of Padua, Padua, in 2010, and the M.Sc. and D.Sc. degrees (both with distinction) in electrical engineering from Aalto University, Espoo, Finland, in 2012 and 2017, respectively. Since 2012, he has been with the Department of Electronics and Nanoengineering, Aalto University, where he is currently a Post-Doctoral Researcher. His expertise is in the field of all-digital RF transmitters, with special focus on the implementation of high-speed DSP algorithms.

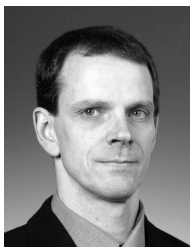

Kari Stadius (S'95–M'03) received the M.Sc., Lic. Tech., and Doctor of Science degrees in electrical engineering from the Helsinki University of Technology, Helsinki, Finland, in 1994, 1997, and 2010, respectively. He is currently working as a staff scientist at the Department of Electronics and Nanoengineering, Aalto University School of Electrical Engineering. His research interests include the design and analysis of RF transceiver blocks with special emphasis on frequency synthesis. He has authored or coauthored over 70 refereed journal and conference papers in the areas of analog and RF circuit design.

Lauri Anttila Lauri Anttila (S'06, M'11) received the M.Sc. degree and the D.Sc. (Tech) degree (with honors) in electrical engineering from Tampere University of Technology (TUT), Tampere, Finland, in 2004 and 2011. Since 2016, he has been a senior research fellow at the Department of Electronics and Communications Engineering at TUT. In 2016-2017, he was a visiting research fellow at the Department of Electronics and Nanoengineering, Aalto University, Finland. His research interests are in signal processing for wireless communications, transmitter and receiver linearization, and radio implementation challenges in 5G cellular radio, full-duplex radio, and large-scale antenna systems. He has co-authored over 70 peer reviewed articles in these areas, as well as three book chapters.

Mikko Valkama (S'99–M'02–SM'15) was born in Pirkkala, Finland, on November 27, 1975. He received the M.Sc. and Ph.D. Degrees (both with honors) in electrical engineering (EE) from Tampere University of Technology (TUT), Finland, in 2000 and 2001, respectively. In 2002, he received the Best Ph.D. Thesis -award by the Finnish Academy of Science and Letters for his dissertation entitled "Advanced I/Q signal processing for wideband receivers: Models and algorithms". In 2003, he was working as a visiting researcher with the Communications Systems and Signal Processing Institute at SDSU, San Diego, CA. Currently, he is a Full Professor and Department Vice-Head at the Department of Electronics and Communications Engineering at TUT, Finland. His general research interests include communications signal processing, estimation and detection techniques, signal processing algorithms for software defined flexible radios, cognitive radio, full-duplex radio, radio localization, 5G mobile cellular radio, digital transmission techniques such as different variants of multicarrier modulation methods and OFDM, and radio resource management for ad-hoc and mobile networks.

Jussi Ryynänen (S'99–M'04–SM'16) was born in Ilmajoki, Finland, in 1973. He received his Master of Science, Licentiate of Science, and Doctor of Science degrees in electrical engineering from Helsinki University of Technology (HUT), Helsinki, Finland, in 1998, 2001, and 2004, respectively. He is currently working as an associate professor at the Department of Electronics and Nanoengineering, Aalto University School of Electrical Engineering. His main research interests are integrated transceiver circuits for wireless applications. He has authored or coauthored over 100 refereed journal and conference papers in the areas of analog and RF circuit design. He holds six patents on RF circuits